Research article

Francisco Freire-Fernández*, Mikko Kataja and Sebastiaan van Dijken*

Surface-plasmon-polariton-driven narrow-linewidth magneto-optics in Ni nanodisk arrays

https://doi.org/10.1515/nanoph-2019-0331
Received August 26, 2019; revised November 18, 2019; accepted November 21, 2019

Abstract: The field of magnetoplasmonics exploits interactions between light and magnetic matter at the nanoscale for light manipulation and resonant magneto-optics. One of the great challenges of this field is overcoming optical losses in magnetic metals. Here, we exploit surface plasmon polaritons (SPPs) excited at the interface of an SiO_2/Au bilayer to induce strong magneto-optical responses on the Ni nanodisks of a periodic array. Using a reference system made of Au nanodisks, we show that optical losses in Ni hardly broaden the linewidth of SPP-driven magneto-optical signals. Loss mitigation is attained because the free electrons in the Ni nanodisks are driven into forced oscillations away from their plasmon resonance. By varying the SiO_2 layer thickness and lattice constant of the Ni nanodisk array, we demonstrate tailoring of intense magneto-optical Kerr effects with a spectral linewidth down to ~25 nm. Our results provide important hints on how to circumvent optical losses and enhance magneto-optical signals via the design of off-resonance magnetoplasmonic driving mechanisms.

Keywords: magnetoplasmonics; nanoparticle array; surface plasmon polariton; surface lattice resonance; magneto-optical Kerr effect.

***Corresponding authors: Francisco Freire-Fernández, and Sebastiaan van Dijken:** NanoSpin, Department of Applied Physics, Aalto University School of Science, P.O. Box 15100, FI-00076 Aalto, Finland, e-mail: francisco.freirefernandez@aalto.fi. https://orcid.org/0000-0002-6539-419X (F. Freire-Fernández); sebastiaan.van.dijken@aalto.fi. https://orcid.org/0000-0001-6372-2252 (S. van Dijken)
Mikko Kataja: NanoSpin, Department of Applied Physics, Aalto University School of Science, P.O. Box 15100, FI-00076 Aalto, Finland; and Institut de Ciència de Materials de Barcelona (ICMAB-CSIC), Campus de la UAB, Bellaterra, Catalonia, Spain

1 Introduction

The integration of plasmonics and magneto-optics has led to the emergence of a new research field known as magnetoplasmonics [1–3]. The main goal of magnetoplasmonics is twofold. First, the use of magnetic materials in plasmonic structures enables active light manipulation at the nanoscale via field-controlled breaking of time-reversal symmetry. Examples include demonstrations of magnetic modulations of the surface plasmon polariton (SPP) wave vector in Au-Co-Au trilayers [4], magneto-optical transparency in magnetoplasmonic crystals [5], and magnetic-field-controlled routing of light emission from diluted-magnetic-semiconductor quantum wells [6]. Second, the excitation of surface plasmons in magnetic materials can be used to resonantly enhance and spectrally tailor their magneto-optical response [7–10]. This configurability is attractive for label-free biosensing [11] and ultrafast all-optical magnetic switching [12].

Despite its promise, the field of magnetoplasmonics faces a challenge of overcoming optical losses [13–15]. This is particularly true for nanostructures containing magnetic metals whose losses are significantly higher than those of noble metals. One of the loss-mitigating strategies in noble-metal plasmonics involves the near- or far-field coupling of nanostructures. In periodic two-dimensional nanoparticle arrays, for instance, radiative coupling between diffracted waves in the array plane and localized surface plasmon resonances (LSPRs) produces collective surface lattice resonances (SLRs) [16–20]. The full width at half maximum (FWHM) of SLRs in Au or Ag nanoparticle arrays can be <10 nm [16, 20], which is significantly smaller than the 80–100 nm FWHM of LSPRs in isolated nanostructures of the same noble metals. Based on these results, it seems logical to transfer the concept of collective resonances as a loss-mitigating mechanism to magnetoplasmonics. Arrays of higher-loss magnetic nanoparticles indeed support SLRs, offering resonant enhancements of the magneto-optical activity [10, 21]. Despite this attractive property, the SLRs of magnetic lattices are typically one order of magnitude broader than those of noble metal systems.

Another loss reduction strategy in magnetoplasmonics involves the integration of noble and magnetic metals. Realizations such as near-field coupled vertical dimers [22–24] and far-field coupled checkerboard patterns [25] show a moderate narrowing of plasmon resonances compared to those in all-magnetic structures. The loss properties of hybrid magnetoplasmonic systems can be understood by considering the coupling of weakly and heavily damped oscillators that are driven near their resonance frequencies by an external force.

A few other options are available to circumvent losses in magnetoplasmonics. For instance, one could refrain from using magnetic metals altogether. Most notably, hybrid structures of noble metals and dielectric iron garnets combine narrow plasmon resonances and strong magneto-optical responses [7, 9]. Magnetic fields can also be drastically enhanced in noble metal split-ring resonators [26] or by coupling of magnetic plasmon resonances to SPPs in such structures [27]. Alternative loss-compensation mechanisms involving magnetic metals include the integration of thin magnetic films with photonic crystals [28] and lasing in magnetic nanodisk arrays overlaid with an organic gain medium [29].

In this work, we demonstrate a hybrid magnetic metal/noble metal magnetoplasmonic structure that avoids the inherently high optical losses of magnetic materials. Our system consists of a square Ni nanodisk array placed onto an SiO_2/Au bilayer. In this configuration, the array acts as a grating coupler for the excitation of spectrally narrow SPPs at the SiO_2/Au interface. The slowly decaying near field of the SPP mode on the dielectric side of the SiO_2/Au interface [30], in turn, drives the free electrons of the Ni nanodisks into forced oscillations away from their resonance frequency. Through electronic spin-orbit coupling in the perpendicularly magnetized Ni nanodisks, this produces an intense magneto-optical Kerr effect in an equally narrow spectral range.

2 Results and discussion

Figure 1A schematically illustrates our magnetoplasmonic structure. The 150-nm-thick Au film is grown by electron beam evaporation onto a glass substrate and is covered by an atomic-layer-deposited SiO_2 film of varying thickness (5–60 nm). On top of this bilayer, the Ni nanodisk arrays are patterned using electron beam lithography. The Ni nanodisks have a diameter of 200 nm and a thickness of 70 nm, and they are arranged into square arrays with a lattice constant (a) ranging from 350 to 500 nm (Figure 1B). As a reference, we made identical all-noble-metal structures by replacing the Ni nanodisks with Au. We also fabricated Co/Pt nanodisk arrays on top of TiO_2/Au bilayers.

We start the discussion of results by considering optical reflectivity measurements. The samples are characterized at normal incidence using linearly polarized light along the x-axis of the nanodisk arrays (Figure 1A). To ensure a homogeneous dielectric environment, we embedded the nanodisks in index-matching oil (refractive

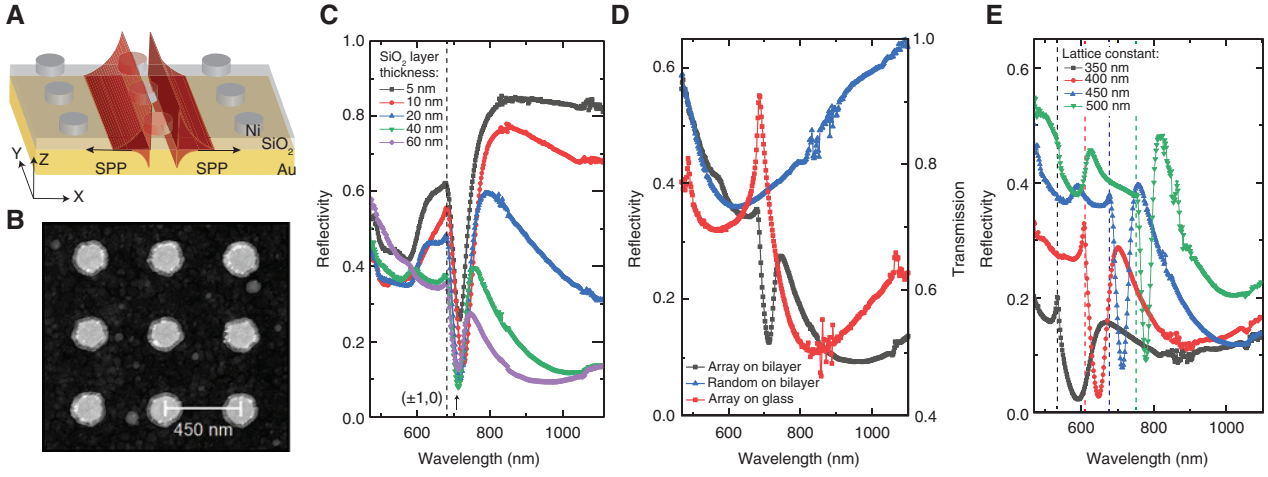

Figure 1: Sample configuration and optical characterization.
(A) Schematic of the magnetoplasmonic sample. (B) Atomic force microscopy image of an Ni nanodisk array on top of an SiO_2/Au bilayer. (C) Optical reflectivity measurements of Ni nanodisk arrays on SiO_2/Au bilayers with $a = 450$ nm and varying SiO_2 thicknesses. (D) Reflectivity spectrum of an Ni nanodisk array on top of a 60-nm SiO_2/Au bilayer and transmission curve of an identical Ni nanodisk array on glass. The lattice constant of the arrays is 450 nm. For comparison, the reflectivity spectrum of randomly distributed Ni nanodisks on an SiO_2/Au bilayer is also shown. (E) Optical reflectivity measurements of Ni nanodisk arrays on SiO_2/Au bilayers with a constant SiO_2 thickness of 40 nm and different lattice constants. The vertical dashed lines in (C) and (E) indicate the (±1, 0) diffracted orders of the Ni nanodisk arrays.

index $n=1.52$). Figure 1C shows the optical reflectivity of square Ni nanodisk arrays on top of SiO_2/Au bilayers. In these measurements, the lattice constant is fixed at 450 nm and the thickness of the SiO_2 is varied from 5 to 60 nm. The reflectivity spectra display maxima at the wavelength of the Rayleigh anomaly, $\lambda_{p,q}=\frac{na}{\sqrt{p^2+q^2}}$, corresponding to the $(p, q)=(\pm1, 0)$ diffracted orders of the Ni nanodisk array, with p and q indicating the order of diffraction along x and y, respectively ($\lambda_{1,0}=684$ nm for $a=450$ nm). If the wave vector of the diffracted waves in the array plane matches that of a plasmon mode at the SiO_2/Au interface, two counterpropagating SPPs are excited. Energy absorption by the SPP mode reduces the reflectivity. Because the wave vectors of the SPPs are given by $k_{SPP}=\pm k_0\sqrt{\frac{\varepsilon_{SiO_2}\cdot\varepsilon_{Au}}{\varepsilon_{SiO_2}+\varepsilon_{Au}}}$, the free space wavelength of an SPP excitation corresponds to [31]

$$\lambda'_{p,q}=\frac{a}{\sqrt{p^2+q^2}}\cdot\sqrt{\frac{\varepsilon_{SiO_2}\cdot\varepsilon_{Au}}{\varepsilon_{SiO_2}+\varepsilon_{Au}}}. \quad (1)$$

Here, k_0 is the wave vector in free space and ε_{SiO_2} and ε_{Au} are the dielectric constants of SiO_2 and Au. Based on Eq. (1) and dielectric constants determined by ellipsometry, we estimate an SPP excitation wavelength of 706 nm at normal incidence. This value is congruent with our measurements indicating a deep minimum in the optical reflectivity spectra at a wavelength of ~710 nm ($a=450$ nm). The resonances labeled by the upward-pointing arrow in Figure 1C thus correspond to the excitation of narrow-linewidth SPPs at the SiO_2/Au interface.

In addition to the SPP mode, the reflectivity spectra of Figure 1C exhibit a second resonance at a larger wavelength. For an SiO_2 thickness of 60 nm, the spectral shape of this feature resembles that of an identical Ni nanodisk array on glass, as illustrated by the data of Figure 1D. In the latter geometry, the resonance at 830 nm corresponds to the excitation of an SLR mode [10, 21]. For the Ni nanodisk array on 60-nm SiO_2/Au, the resonance wavelength is shifted to 940 nm and it redshifts further for thinner SiO_2 layers (see Figure 1C). Simultaneously, the resonance mode loses intensity. Both effects are explained by the formation of image dipoles in the Au film if the SiO_2 layer is thin, as discussed previously for noble-metal plasmonic systems [32–37]. The collective nature of the plasmon resonance mode in the Ni nanodisk arrays on top of SiO_2/Au bilayers is confirmed further by the distinct optical response of randomly distributed Ni nanodisks on SiO_2/Au (blue curve in Figure 1D). In the latter case, the broad resonance centered at ~620 nm corresponds to the LSPR mode of individual Ni nanodisks. Once placed in a periodic array, the LSPRs couple and the resonance wavelength redshifts. Hereafter, we refer to this collective resonance as the SLR-related mode.

Figure 1E summarizes the dependence of the optical reflectivity spectra on the lattice constant for a fixed SiO_2 thickness of 40 nm. As anticipated, the SPP and SLR-related modes shift to larger wavelength when the (±1, 0) diffracted order moves up. The reflectivity minima closely follow the SPP excitation wavelength given by Eq. (1) for all samples. An increase of the lattice constant from 350 to 500 nm narrows the SPP resonance. For $a=500$ nm, the SPP resonance in the reflectivity spectrum has an FWHM of 25 nm.

We now address the optical losses in our hybrid magnetoplasmonic structure. As already pointed out, the introduction of magnetic metals into noble-metal plasmonic systems tends to broaden the resonances because of mode hybridization [22–25]. Coupling between the narrow-linewidth SPP mode and the broader plasmon resonance on the Ni nanodisks could have a similar effect. To investigate the potentially detrimental role of optical losses in Ni, we fabricated identical samples with Au nanodisks. Figure 2A shows the optical reflectivity of the

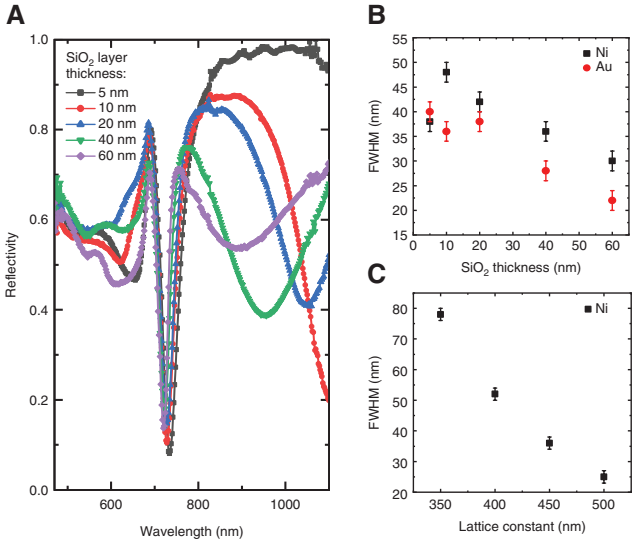

Figure 2: Comparison of all-noble-metal and hybrid magnetoplasmonic structures.
(A) Optical reflectivity measurements of Au nanodisk arrays on SiO_2/Au bilayers with $a=450$ nm and varying SiO_2 thicknesses. (B) FWHM of the SPP mode in reflectivity spectra of Ni and Au nanodisk arrays with $a=450$ nm on SiO_2/Au bilayers with varying SiO_2 thicknesses. (C) Dependence of the SPP resonance linewidth on the lattice constant for Ni nanodisk arrays on SiO_2/Au. The SiO_2 layer thickness is 40 nm.

reference structures with $a = 450$ nm and different SiO_2 thicknesses. The spectra resemble those of the samples with Ni nanodisks depicted in Figure 1C. Particularly, the FWHM of the SPP resonances in the reflectivity spectra is similar for both plasmonic systems (Figure 2B). This weak dependence on material demonstrates that the SPP and localized mode do not significantly hybridize. Optical losses in the Ni nanodisks, therefore, do not affect the SPPs much. Figure 2B summarizes the FWHM of the SPP resonance as a function of SiO_2 thickness in both systems, and Figure 2C depicts its dependence on lattice constant for the Ni nanodisk samples. We note that the minor effect of optical losses in the Ni nanodisks on the SPP linewidth is universal. To illustrate this further, we fabricated arrays of Co/Pt nanodisks on top of TiO_2/Au bilayers. The results shown in Figure S1 of the Supplementary Material indicate that SPP resonances with an FWHM down to ~25 nm are attained for $a = 450$ nm and $t_{TiO_2} = 30$ nm, which compare well to the data for the Ni and Au nanodisk samples (Figure 2B).

Figure 3 depicts how the excitation of plasmon resonances translates to the magneto-optical activity of the Ni nanodisk samples. In (A) and (B), we plot the polar Kerr rotation (θ) and Kerr ellipticity (ε) for square nanodisk arrays with $a = 450$ nm and different SiO_2 thicknesses, i.e. the same samples as in Figure 1C. Both parameters are measured simultaneously using a photoelastic modulator and lock-in detection (see Section 4). Additionally, we plot the Kerr angle $\Phi = \sqrt{\theta^2 + \varepsilon^2}$ in Figure 3C. The measurements reveal that the SPPs at the SiO_2/Au interface produce an intense and narrow-linewidth magneto-optical signal. At the SPP wavelength of ~710 nm, the Kerr rotation peaks and the Kerr ellipticity changes sign.

To rationalize the magneto-optical response, one has to consider how the optical near field of the leaky SPP mode drives the free electrons of the Ni nanodisks into forced oscillations. The forced oscillations produce an electric dipole along the x-axis (p_x). Because we saturate the Ni magnetization perpendicular to the sample plane by an external magnetic field, electronic spin-orbit coupling within the Ni nanodisks produces a second electric dipole along the y-axis (p_y) [8]. The real and imaginary parts of the ratio between scattered fields along the y- and x-axis determine the Kerr rotation and Kerr ellipticity, respectively. Because of the phase dependence of these forced oscillations, the Kerr rotation and Kerr ellipticity signals in Figure 3A,B are spectrally narrower than the SPP resonances in the reflectivity measurements of Figure 1C (this is particularly true for the Kerr rotation). In contrast, the FWHM of SPP-driven resonances in the Kerr angle spectra are comparable to the reflectivity data. Figure 3D summarizes the linewidth of the SPP-driven magneto-optical signals.

The magnitude of the Kerr angle at the SPP wavelength is the largest for 10–40-nm SiO_2 and drops when the Ni nanodisks are placed 60 nm above the SiO_2/Au interface (Figure 3C). The evanescent confinement of the SPP mode explains this fall off [30]. We also note a reduction of the Kerr signal for 5-nm SiO_2, which correlates with an increase in optical reflectivity (Figure 1C). This points to a weakening of the SPP-driven electric dipole on the Ni nanodisks when the SiO_2 layer is very thin. Screening of

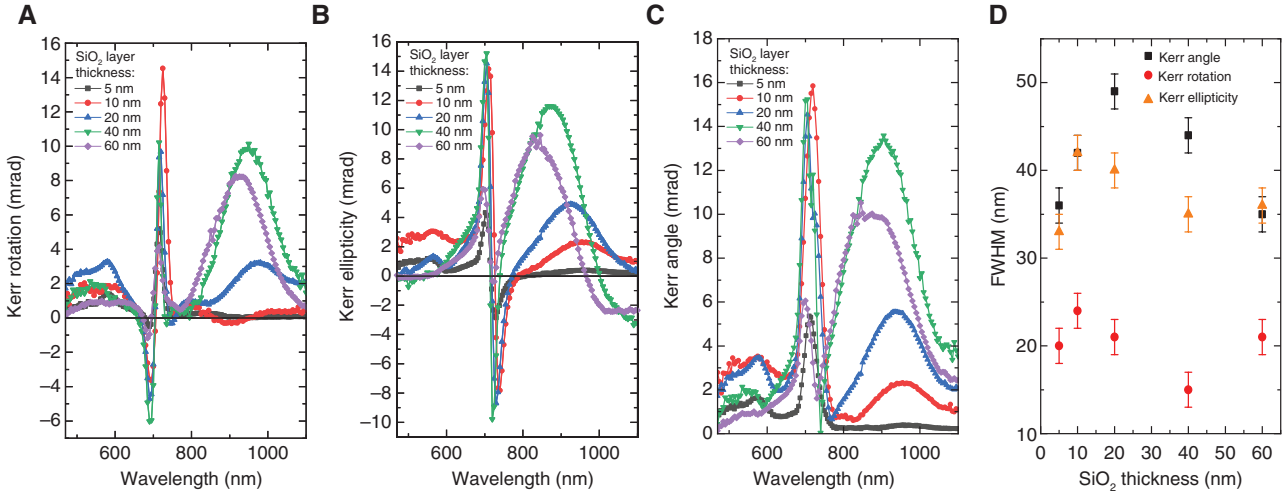

Figure 3: Magneto-optical characterization of the samples.
(A–C) Magneto-optical Kerr rotation, Kerr ellipticity, and Kerr angle of Ni nanodisk arrays on SiO_2/Au bilayers with $a = 450$ nm and varying SiO_2 thicknesses. (D) FWHM of the SPP-driven resonance in the magneto-optical spectra of (A) to (C).

the electric dipole by the Au film, which is most efficient at a small SiO_2 thickness, explains this effect. Besides the SPP resonance, the broader SLR-related mode also tailors the magneto-optical response (Figure 3C). As the electric dipoles on the Ni nanodisks are primarily driven by the incident light at larger wavelengths, the dependence of the Kerr angle on SiO_2 thickness is different for this mode. The formation of image dipoles in the Au film almost completely suppresses the magneto-optical response at the SLR-related wavelength for 5-nm SiO_2. Beyond this, the Kerr signal first increases to a maximum at $t_{SiO_2} = 40$ nm before declining again. The latter observation indicates that placing Ni nanodisk arrays onto an optimized dielectric/metal bilayer enhances their magneto-optical signal compared to an identical array on glass. We discuss this comparison in more detail later. Magneto-optical data for samples with varying lattice constants corroborate the main findings (Figures S2 and S3, Supplementary Material).

Finite-difference time-domain (FDTD) simulations in Lumerical software (Lumerical Inc., Vancouver, Canada) support our experimental results. In the simulations, we irradiated a 3×3 nanodisk array on top of an SiO_2/Au bilayer under periodic boundary conditions. This structure was excited at normal incidence by a linearly polarized plane wave with the electric field aligned along the *x*-axis (see Section 4). Figure 4A compares reflectivity spectra for Ni nanodisk arrays on SiO_2/Au bilayers with $a = 450$ nm and 10- or 40-nm SiO_2. The simulated curves reproduce the main features of the experimental resonances. To visualize the distribution of electric fields at the resonance wavelengths, we placed an *xy* monitor right on top of the Ni nanodisks and *xz* and *yz* monitors intersecting the disks (see Figure 4B). The monitors record two field contributions at the SPP wavelength (λ_1), the propagating SPPs, and a localized mode on the Ni nanodisks. The SPP-driven electric dipoles on the Ni nanodisks have similar intensities for 10-nm SiO_2 and 40-nm SiO_2 (Figure 4C–E) and, through the spin-orbit

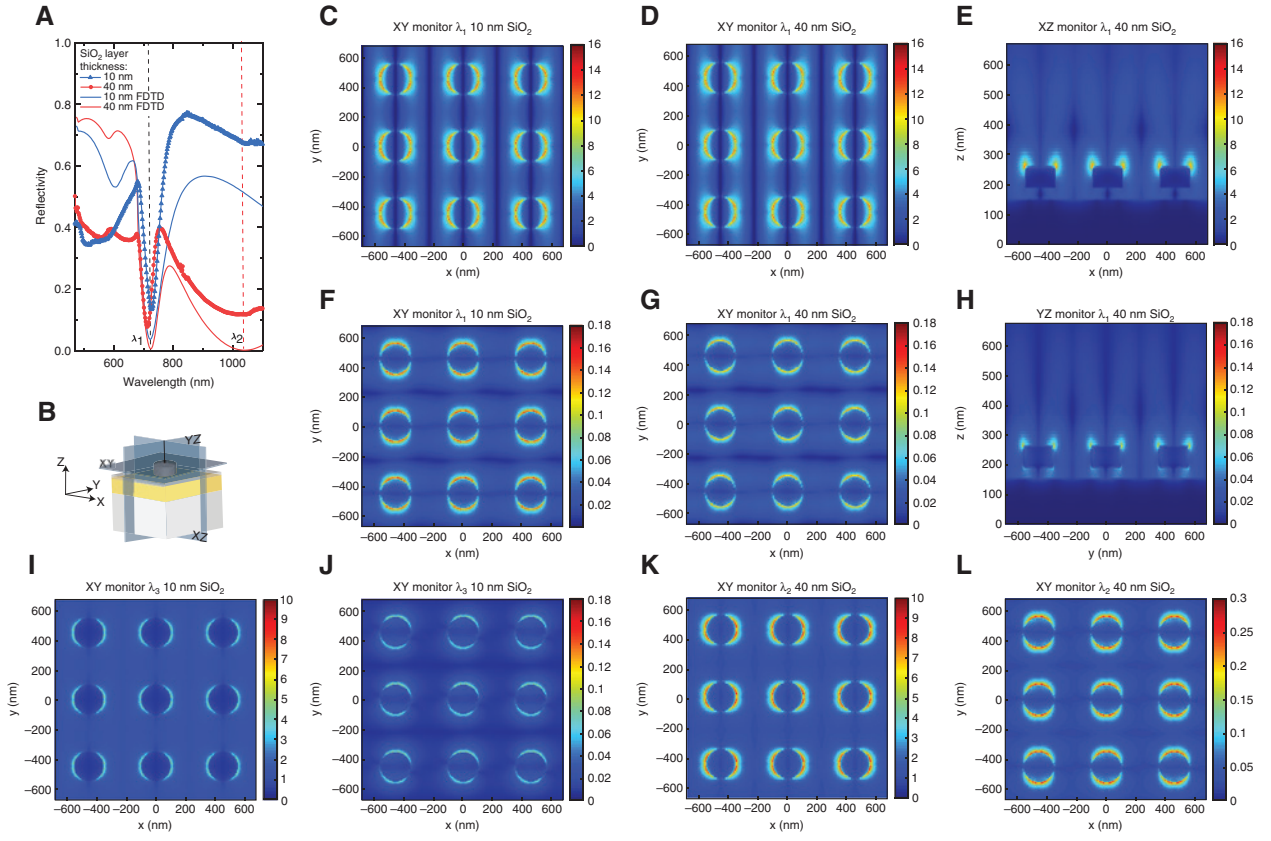

Figure 4: FDTD simulations of the magnetoplasmonic samples.
(A) Comparison of simulated and measured reflectivity spectra of Ni nanodisk arrays on SiO_2/Au bilayers with $a = 450$ nm and SiO_2 thicknesses of 10 and 40 nm. (B) Schematic of the monitors used to visualize the distribution of electric fields in different planes of the sample. (C–E) Electric field distribution at the SPP wavelength (λ_1) for samples with 10-nm SiO_2 and 40-nm SiO_2. (F–H) Field distribution of the orthogonal electric dipoles at λ_1 that are induced by spin-orbit coupling within the Ni nanodisks. (I–L) Electric field distribution of the two orthogonal dipoles at the SLR-related resonance wavelength for samples with 10-nm SiO_2 ($\lambda_3 = 1385$ nm) and 40-nm SiO_2 ($\lambda_2 = 1100$ nm).

coupling, this also produces similar electric dipoles along the *y*-axis of the disks (Figure 4F–H). The simulated electric field strengths explain the large magneto-optical Kerr effect at the SPP wavelength of the corresponding experimental samples (Figure 3A–C), as demonstrated for 10-nm SiO_2 in Figure S4 of the Supplementary Material. For comparison, we also simulated the distribution of electric fields at the wavelength of the Rayleigh anomaly (Figure S5, Supplementary Material). The simulations clearly show that the electric dipoles on the Ni nanodisks are suppressed substantially at the diffracted order of the array, limiting the magneto-optical response just before the SPP mode. At the SLR-related resonance wavelength (Figure 4I–L), the simulated electric fields are stronger for 40-nm SiO_2 than 10-nm SiO_2, in agreement with the experimental Kerr effect data. FDTD simulations for Ni nanodisk arrays on SiO_2/Au bilayers with an SiO_2 thickness of 5 nm are shown in Figure S6 of the Supplementary Material.

The effect of optical losses in the Ni nanodisks on the resonance properties of the SPP-driven electric dipole can be understood qualitatively by considering two coupled oscillators (Figure S7, Supplementary Material). One of the oscillators represents the surface plasmon mode on the Ni nanodisks. Coupling between single-particle LSPRs and the diffracted order of the periodic array plus the formation of image dipoles in the Au layer determine the resonance properties of this mode. In the reflectivity spectra, this produces the SLR-related resonance at a large wavelength. The second oscillator represents the SPP mode that is excited at the SiO_2/Au interface. If the resonance frequencies of the two oscillators are different, the SPP oscillator induces a narrow resonance on the Ni nanodisk oscillator. Importantly, the linewidth of this forced oscillation does not depend on the damping parameter of the driven oscillator (Figures S8 and S9, Supplementary Material). This condition is met in our hybrid magnetoplasmonic structures because of the clear spectral separation between the SPP and SLR-related resonances. In other words, off-resonance driving of the Ni nanodisk array by the near field of a spectrally narrow SPP mode is hardly affected by the optical losses of Ni. For other hybrid magnetoplasmonic systems comprising noble and magnetic metals, the situation is often different. We illustrate this by considering vertical dimers and checkerboard arrays. In vertical dimers, two metal nanodisks of similar size couple via optical near fields. The LSPRs of magnetic nanodisks are particularly broad, making a spectral overlap of the two resonance modes in magnetoplasmonic dimers inevitable. In checkerboard arrays, lower- and higher-loss metal nanodisks couple via optical far fields. In both geometries, the noble metal and magnetic subsystems can be represented by two coupled oscillators that are driven on-resonance (or close to resonance) by an external electric field. This leads to mode hybridization and linewidth broadening, the extent of which depends on the damping parameter of both oscillators (Figure S8, Supplementary Material).

To put our results into further perspective, we conclude this work by comparing different Ni nanodisk structures with identical shape, size, and packing density (Figure 5). For a random distribution of Ni nanodisks, the broad LSPR produces a weak and broad Kerr signal [8]. Ordering of the Ni nanodisks into a periodic array on glass enhances the Kerr angle through the excitation of a collective SLR [10, 21]. The FWHM of the SLR mode is, however, broad (~200 nm). Placing the same Ni nanodisk array on an SiO_2/Au bilayer generates two main resonances in the magneto-optical spectrum: one broad SLR-related mode and a narrow SPP-driven mode. The intensities of both resonances can be tailored to about three times the signal of the Ni nanodisk array on glass by variation of the SiO_2 thickness (Figure 3). The narrow linewidth of the SPP-driven mode is particularly interesting for label-free biosensing. The figure-of-merit (FoM) of a plasmonic sensor is often defined as the product of sensitivity (shift in resonance wavelength upon a change of the surrounding refractive index) and the resonance linewidth [38, 39]. In magnetoplasmonic biosensing,

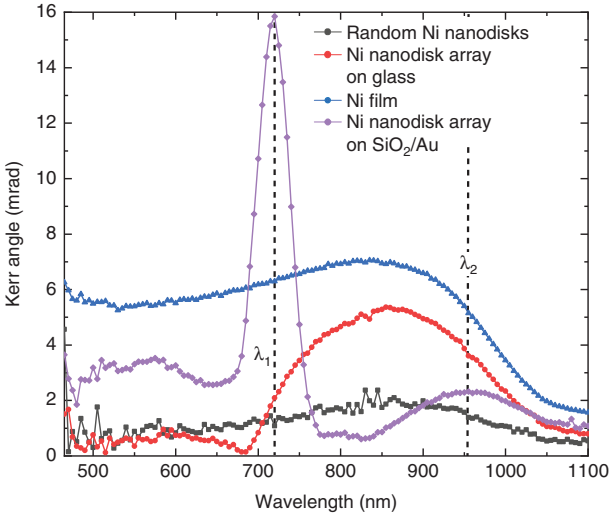

Figure 5: Magneto-optical Kerr angle measured on a random distribution of Ni nanodisks (black squares), a continuous 70-nm-thick Ni film (blue triangles), an Ni nanodisk array on glass (red dots), and an Ni nanodisk array on an SiO_2/Au bilayer (purple diamonds). The Ni nanodisks are 70 nm thick and their diameter is 200 nm. The lattice constant of the arrays is 450 nm. The SiO_2 thickness is 10 nm.

refractive index changes are detected by monitoring the wavelength where the Kerr rotation or Kerr ellipticity crosses zero [11, 40, 41]. The measurement accuracy, therefore, depends on the slope $d\theta/d\lambda$ or $d\varepsilon/d\lambda$ at the nulling condition. As outlined for randomly distributed Ni nanodisks in Ref. [11], phase-sensitive detection of the Kerr ellipticity nulling condition already provides a large enhancement of the refractometric sensing FoM. The sharp spectral features in the magneto-optical spectra of the samples presented here would further increase the sensing performance by an estimated one to two orders of magnitude. Moreover, efficient time-reversal symmetry breaking in Ni nanodisk arrays on SiO_2/Au may be used to lift the degeneracy of plasmon modes at high-symmetry points of the Brillouin zone [42], which could lead to topological photonic effects.

3 Conclusions

In summary, we demonstrated narrow-linewidth magneto-optical Kerr signals by placing Ni nanodisk arrays within the optical near field of SPPs at the interface of an SiO_2/Au bilayer. The low-loss magneto-optical resonances are explained by SPP-driven forced oscillations of free electrons and spin-orbit coupling in the Ni nanodisks. The wavelength and magnitude of the Kerr angle can be tailored by variation of the lattice constant and thickness of the SiO_2 layer.

4 Methods

4.1 Sample fabrication

The samples were fabricated on glass substrates using electron beam evaporation for the 150-nm-thick Au film and atomic layer deposition (ALD) for the SiO_2 layer. ALD was performed at 120°C in a FTS 500 plasma system (Beneq Oy, Espoo, Finland). The dielectric constants of the Au and SiO_2 films were measured using an ellipsometer (J.A. Woollam Inc., Lincoln, NE, USA). On top of the SiO_2/Au bilayers, the Ni nanodisk arrays were patterned using an electron beam lithography process in a EPBG5000pES system (Vistec Electron Beam GmbH, Jena, Germany). After patterning of the Poly(methyl methacrylate) resist layer, 70 nm of Ni was grown by electron beam evaporation and lift-off in acetone. For the reference samples, we used the same process with Au. We also fabricated Co/Pt nanodisks arrays on top of TiO_2/Au bilayers.

4.2 Optical and magneto-optical measurements

For sample characterization, we used a magneto-optical Kerr spectrometer. The setup consisted of a supercontinuum laser (SuperK EXW-12 laser with acousto-optical filter from NKT Photonics, Birkerød, Denmark), polarizing and focusing optics, a photoelastic modulator (Hinds Instruments I/FS50, Portland, OR, USA), and a photodetector. The wavelength of the laser was tuned between 475 and 1100 nm. We used linearly polarized light at normal incidence with the electric field aligned along the x-axis of the sample. During measurements, a ±400 mT field from an electromagnet switched the magnetization of the Ni nanodisks between the two perpendicular directions. The magneto-optical Kerr rotation and ellipticity were simultaneously recorded by lock-in amplification of the modulated signal at 50 and 100 kHz. The optical reflectivity was determined using $R = 1 - \frac{I_{\mathrm{ref}} - I}{I_{\mathrm{ref}} - I_d}$, where I and I_{ref} are the reflected light intensities from the nanodisk array and an area without nanodisks, respectively, and I_d is the dark current of the photodetector. All measurements were performed with the Ni, Au, or Co/Pt nanodisks immersed in index-matching oil with $n = 1.52$. We note that similar results would be obtained if an SiO_2 capping layer replaces the index-matching oil [29].

4.3 FDTD simulations

Commercial Lumerical FDTD software was used to simulate the optical response of the magnetoplasmonic system. Magneto-optical effects were included in the simulations by following the procedure given in Ref. [43]. For the material parameters of Ni and Au, we used data from Refs. [44] and [45], respectively. Only the Ni nanodisks were assumed to be magneto-optically active and contain off-diagonal permittivity tensor elements. We simulated 3×3 nanodisks on top of an SiO_2/Au bilayer and used periodic boundary conditions at the edges of the simulation area to mimic an extended array. The diameter and thickness of the Ni nanodisks and the thicknesses of the SiO_2 and Au layers were set to the experimental values. Moreover, the nanodisks were assumed to be surrounded by an index-matching environment ($n = 1.52$). The sample was excited at normal incidence by a linearly

polarized plane wave with the electric field aligned along the x-axis. The orthogonal electric dipoles depicted in Figure 4F–H,J,L were obtained by subtracting the simulation data for two perpendicular magnetization directions, which was implemented by exchanging the signs of the off-diagonal terms in the Ni dielectric tensor. Excitation of these orthogonal dipoles via spin-orbit coupling inside the Ni nanodisks produces the magneto-optical Kerr effect. Magneto-optical Kerr angles were obtained by projecting the simulated electric fields into the far field using the built-in tools of the Lumerical FDTD software and integrating the results over a cone of 5° (±2.5° from normal incidence). This procedure yields E_x and E_y, i.e. the electric field components of the reflected beam in the far field. The Kerr angle is given by $|E_y/E_x|$ for x-polarized incident radiation.

Acknowledgments: This work was supported by the Academy of Finland under Project No. 316857, Funder Id: http://dx.doi.org/10.13039/501100002341 and by the Aalto Centre for Quantum Engineering. M.K. acknowledges support from the European Commission (Marie Skłodowska-Curie IF EMPHASIS – DLV-748429). Lithography was performed at the Micronova Nanofabrication Centre, supported by Aalto University.

References

[1] Armelles G, Cebollada G, García-Martín A, González MU. Magnetoplasmonics: combining magnetic and plasmonic functionalities. Adv Opt Mater 2013;1:10–35.
[2] Bossini D, Belotelov VI, Zvezdin AK, Kalish AN, Kimel AV. Magnetoplasmonics and femtosecond optomagnetism at the nanoscale. ACS Photonics 2016;3:1385–400.
[3] Floess D, Giessen H. Nonreciprocal hybrid magnetoplasmonics. Rep Prog Phys 2018;81:116401.
[4] Temnov VV, Armelles G, Woggon U, et al. Active magneto-plasmonics in hybrid metal-ferromagnet structures. Nat Photonics 2010;4:107–11.
[5] Belotelov VI, Kreilkamp LE, Akimov IA, et al. Plasmon-mediated magneto-optical transparency. Nat Commun 2013;4:2128.
[6] Spitzer F, Poddubny AN, Akimov IA, et al. Routing the emission of a near-surface light source by a magnetic field. Nat Phys 2018;14:1043–8.
[7] Belotelov VI, Akimov IA, Pohl M, et al. Enhanced magneto-optical effects in magnetoplasmonic crystals. Nat Nanotechnol 2011;6:370–6.
[8] Maccaferri N, Berger A, Bonetti S, et al. Tuning the magneto-optical response of nanosize ferromagnetic Ni disks using the phase of localized plasmons. Phys Rev Lett 2013;111:167401.
[9] Chin JY, Steinle T, Wehlus T, et al. Nonreciprocal plasmonics enables giant enhancement of thin-film Faraday rotation. Nat Commun 2013;4:1599.
[10] Kataja M, Hakala T, Julku A, Huttunen MJ, van Dijken S, Törmä P. Surface lattice resonances and magneto-optical response in magnetic nanoparticle arrays. Nat Commun 2015;6:7072.
[11] Maccaferri N, Gregorczyk K, de Oliveira T, et al. Ultrasensitive and label-free molecular-level detection enabled by light phase control in magnetoplasmonic nanoantennas. Nat Commun 2015;6:6150.
[12] Kataja M, Freire-Fernández F, Witteveen J, Hakala TK, Törmä P, van Dijken S. Plasmon-induced demagnetization and magnetic switching in nickel nanoparticle arrays. Appl Phys Lett 2018;112:072406.
[13] Khurgin JB, Boltasseva A. Reflecting upon the losses in plasmonics and metamaterials. MRS Bull 2012;37:768–79.
[14] Khurgin JB. How to deal with the loss in plasmonics and metamaterials. Nat Nanotechnol 2015;10:2–6.
[15] Boriskina SV, Cooper TA, Zeng L, et al. Losses in plasmonics: from mitigating energy dissipation to embracing loss-enabled functionalities. Adv Opt Photon 2017;9:775–827.
[16] Shengli Z, Janel N, Schatz GC. Silver nanoparticle array structures that produce remarkably narrow plasmon lineshapes. J Chem Phys 2004;120:10871–975.
[17] Kravets VG, Schedin F, Grigorenko AN. Extremely narrow plasmon resonances based on diffraction coupling of localized plasmons in arrays of metallic nanoparticles. Phys Rev Lett 2008;101:087403.
[18] Auguié B, Barnes WL. Collective resonances in gold nanoparticle arrays. Phys Rev Lett 2008;101:143902.
[19] Khlopin D, Laux F, Wardley WP, et al. Lattice modes and plasmonic linewidth engineering in gold and aluminum nanoparticle arrays. J Opt Soc Am B 2017;34:691–700.
[20] Kravets VG, Kabashin AV, Barnes WL, Grigorenko AN. Plasmonic surface lattice resonances: a review of properties and applications. Chem Rev 2018;118:5912–51.
[21] Maccaferri N, Bergamini L, Pancaldi M, et al. Anisotropic nanoantenna-based magnetoplasmonic crystals for highly enhanced and tunable magneto-optical activity. Nano Lett 2016;16:2533–42.
[22] Banthí JC, Meneses-Rodríguez D, García F, et al. High magneto-optical activity and low optical losses in metal-dielectric Au/Co/Au-SiO_2 magnetoplasmonic nanodisks. Adv Mater 2012;24:OP36–41.
[23] Armelles G, Cebollada A, García-Martín A, et al. Mimicking electromagnetically induced transparency in the magneto-optical activity of magnetoplasmonic nanoresonators. Opt Express 2013;21:27356.
[24] de Sousa N, Froufe-Pérez LS, Armelles G, et al. Interaction effects on the magneto-optical response of magnetoplasmonic dimers. Phys Rev B 2014;89:205419.
[25] Kataja M, Pourjamal S, Maccaferri N, et al. Hybrid plasmonic lattices with tunable magneto-optical activity. Opt Express 2016;24:3652–62.
[26] Chen J, Fan W, Zhang T, et al. Engineering the magnetic plasmon resonances of metamaterials for high-quality sensing. Opt Express 2017;25:3675–81.
[27] Chen J, Nie H, Peng C, et al. Enhancing the magnetic plasmon resonance of three-dimensional optical metamaterials via strong coupling for high-sensitivity sensing. J Lightwave Technol 2018;36:3481–5.
[28] Ignatyeva DO, Knyazev GA, Kapralov PO, Dietler G, Sekatskii SK, Belotelov VI. Magneto-optical plasmonic heterostructure

with ultranarrow resonance for sensing applications. Sci Rep 2016;6:28077.
[29] Pourjamal S, Hakala TK, Necada M, et al. Lasing in Ni nanodisk arrays. ACS Nano 2019;13:5686–92.
[30] Barnes WL, Dereux A, Ebbesen TW. Surface plasmon subwavelength optics. Nature 2003;424:824–30.
[31] Papanikolaou N. Optical properties of metallic nanoparticle arrays on a thin metallic film. Phys Rev B 2007;75:235426.
[32] Holland WR, Hall DG. Frequency shifts of an electric-dipole resonance near a conducting surface. Phys Rev Lett 1984;52:1041–4.
[33] Nordlander P, Prodan E. Plasmon hybridization in nanoparticles near metallic surfaces. Nano Lett 2004;4:2209–13.
[34] Le F, Lwin NZ, Steele JM, Käll M, Halas NJ, Nordlander P. Plasmons in the metallic nanoparticle-film system as a tunable impurity problem. Nano Lett 2005;5:2009–13.
[35] Noguez C. Surface plasmons on metal nanoparticles: the influence of shape and physical environment. J Phys Chem C 2007;111:3806–19.
[36] Mock JJ, Hill RT, Degiron A, Zauscher S, Chilkoti A, Smith DR. Distance-dependent plasmon resonant coupling between a gold nanoparticle and gold film. Nano Lett 2008;8:2245–52.
[37] Hu M, Ghoshal A, Marquez M, Kik PG. Single particle spectroscopy study of metal-film-induced tuning of silver nanoparticle plasmon resonances. J Phys Chem C 2010;114:7509–14.
[38] Mayer KM, Hafner JH. Localized surface plasmon resonance sensors. Chem Rev 2011;111:3828–57.
[39] Špačková B, Wrobel P, Bocková M, Homola J. Optical biosensors based on plasmonic nanostructures: a review. Proc IEEE 2016;104:2380–408.
[40] Pourjamal S, Kataja M, Maccaferri N, Vavassori P, van Dijken S. Hybrid Ni/SiO_2/Au dimer arrays for high-resolution refractive index sensing. Nanophotonics 2018;7:905–12.
[41] Tran VT, Kim J, Tufa LT, Oh S, Kwon J, Lee J. Magnetoplasmonic nanomaterials for biosensing/imaging and in vitro/in vivo biousability. Anal Chem 2018;90:225–39.
[42] Guo R, Necada M, Hakala TK, Väkeväinen AI, Törmä P. Lasing at K points of a honeycomb plasmonic lattice. Phys Rev Lett 2019;122:013901.
[43] Lumerical. Magneto-optical Kerr effect. Available at: https://apps.lumerical.com/other_application_magneto-optical_kerr_effect.html. Accessed: 2 Dec 2019.
[44] Krinchik GS, Artemjev VA. Magneto-optic properties of nickel, iron, and cobalt. J Appl Phys 1968;39:1276–8.
[45] Johnson PB, Christy RW. Optical constants of the noble metals. Phys Rev B 1972;6:4370–9.

Supplementary Material: The online version of this article offers supplementary material (https://doi.org/10.1515/nanoph-2019-0331).